

The Biological Shield of a High Intensity Spallation Source: a Monte Carlo Design Study

I. Koprivnikar¹, and E. Schachinger
**Institute for Theoretical Physics
Technische Universität Graz*

Abstract

The design of high intensity spallation sources requires best possible estimates for the biological shield. We discuss the layout of the target station shield using Monte Carlo simulation techniques. In order to achieve reasonable computing times together with acceptable accuracy biasing techniques are to be employed and it is the main purpose of this study to develop a calculational strategy for a 3D-Monte Carlo simulation in effective shielding design. Two transport codes, MCNPX and FLUKA, are then applied to the same model spallation source (the European Spallation Source) and results are compared.

Keywords: *Spallation source shielding, Monte Carlo, particle transport*

I. Introduction

Spallation, the bombardment of a heavy metal target by an intense proton beam has become an important technique for the production of high intensity neutron flux. Several new projects for high intensity spallation sources [Spallation Neutron Source (SNS) [1] in the USA, European Spallation Source (ESS) [2] in the EU and the Neutron Science Project (NSP) [3] at JEARl in Japan] are all based on neutron production by means of a high intensity proton beam with proton energies typically in the range of 1 to 2 GeV and beam powers of at least 1 MW. These new conditions require to reinvestigate numerical methods applied so far in the design of the biological shield of the target station. It is expected that a careful design will result in an optimal layout of the shielding and the instrumentation around the target-moderator-reflector complex (TMRC) by reducing the beam lines to minimum length under the required shield design criteria. Furthermore, the shielding costs of the spallation source comprise a significant part of the total facility costs.

Intrinsic to the simulation of radiation transport through a bulk-biological shield, heterogeneous in material, are accuracy problems as a radiation flux attenuation over several orders of magnitude are to be traced by the computer code. In the TMRC of the spallation source neutrons are produced within an energy spectrum which covers 14 decades. In addition, secondary protons and photons will also be generated but they constitute mainly a problem of little importance compared to the shielding problems which are connected with deeply penetrating high energy neutrons as long as a typical multi-layered shield of iron followed by concrete is investigated. These neutrons have a strong angular dependence and can, in the forward direction with respect to the proton beam, reach the energy level of the incident protons. They also cause nucleon-nucleon spallation processes deeply inside the

* A-8010 Graz, Petersgasse 16

¹ Corresponding author, Tel. +43 316 8738686, Fax. +43 316 8738699, E-mail: koprivnikar@itp.tu-graz.ac.at

shield which additionally complicate its design. Neutrons are attenuated by elastic and inelastic scattering, and below the lowest threshold energy for inelastic scattering (the pion production threshold is about 290 MeV) they can build up and penetrate the shield in large numbers. Thus, high energy neutrons in forward direction constitute the most important problem in shielding design.

There are, in principle, two methods which can be employed in shielding design. The classical methods are based on the discrete ordinate expansion of the transport equations [4] or on semi-empirical algorithms based on the Moyer Model [5], and, on the other hand, methods based on Monte Carlo (MC) simulation. The latter are about to become a method of great importance due to the implementation of variance reduction techniques, but also due to the increased speed and memory capacity of the modern computer technology. The obvious advantages of MC simulations are: (i) the particles, their spectra and distributions in the complicated geometry of the TMRC which serves as the particle source for the bulk shielding calculations can be precisely calculated, (ii) charged particles and photons can be treated within one run, (iii) the shield with its beam lines, holes, and narrow gaps which give rise to radiation leaks can be modeled in necessary detail, (iv) energy deposition, material damage and activation can be determined, (v) it is possible to study time dependent processes, and (vi) no high energy cross-section library which is material dependent is required.

It is the aim of this paper to develop a strategy for the design of the biological shield of a high intensity spallation source using as an example the TMRC and the surrounding shielding structure of the European Spallation Source (ESS). Particular emphasis is on the application of variance reducing methods as they are available in the two most prominent MC computer transport codes, namely MCNPX [6] and FLUKA99 [7]. These two codes use different hadron event generators and the low energy transport ($< 150\text{MeV}$) uses different cross-section libraries and methods. A comparison between the results generated by MCNPX and FLUKA will, therefore, also be a prominent part of this paper.

In Section II we concentrate on the simulation of the particles and their energy spectra as they are generated by the TMRC. Using these results as particle source, Section III develops the necessary strategies which will allow a shielding design with Monte Carlo within reasonable time and with necessary accuracy. Finally, conclusions are drawn in Section IV.

II. The TMR-Complex as Secondary Particle Source

The TMRC of a typical high intensity spallation source consists of a liquid-metal target (mercury is the main candidate), a target container built of stainless steel, a number of moderators, all incased by a cooled reflector. To calculate the secondary particles and their energy spectra as they are leaking through the outer TMRC surface, a simple cylindrical model describing the gross features of the TMRC was developed. Fig. 1 presents a view of the TMRC geometry based on the preliminary design parameters of ESS [2]. The target is of slab type and has a curved front end. It is 14 cm high and 30 cm wide in the interaction region. We also added, for completeness, four ambient water moderators, two on top and two below the target, they are of dimension $12 \times 15 \times 5 \text{ cm}^3$ and they serve three beam channels which split into 18 beam lines. The moderator case consists of aluminum, 3 mm thick. Finally, the reflector has a diameter of 150 cm and is 120 cm high. It consists of lead rods which are cooled by heavy water. This heterogeneous reflector structure was homogeneously approximated so as to conserve the number of atoms and the average atomic density for representative materials.

The target is hit by a monoenergetic proton beam of 1.334 GeV within an elliptic cross section of 6 cm vertical axis and 20 cm horizontal axis. Using the LAHET [8] / MCNP [9] code merger MCNPX (version 2.1.5) [6], the angular distribution and the energy spectrum of the hadron leakage (due to the spallation processes in the target region) through the surface of the TMRC have been calculated. The pre-equilibrium model [10] which describes the situation after the intranuclear cascade was set active in all calculations. Thus, an analog simulation of the multi particle transport is performed and a detailed description of the nucleon-meson cascade is obtained. As low energy hadrons generated in the immediate vicinity of the TMRC are of little importance for the layout of the biological shield, this calculation has a low energy cutoff of 1 MeV for neutrons and 10 MeV for charged hadrons. The MCNPX code uses the Bertini-model [11] in the high energy regime and below 150 MeV the continuous nuclear data library LA150 [12] is applied to generate the required cross sections.

Fig. 2 presents the energy spectrum of the hadrons leaking through the TMRC cylindrical surface at the target level in various directions relative to the incident proton beam (0 degrees). For angular resolution a 30 degrees interval has been chosen. The hadrons have been scored using a surface current tally and the cylindrical reflector surface was segmented into scoring zones 40 cm high. The data are normalized to one incident proton and presented per unit lethargy and per unit area. Fig. 3a supplements the detailed results of Fig. 2 presenting a 3-dimensional plot of the energy spectrum of neutrons escaping the TMRC surface in an angular interval from 0 to 180 degrees relative to the incident proton beam. Moreover, Fig. 3b demonstrates a mesh tally depiction of the neutron flux density distribution for energies >10 MeV important for the shielding design in the transverse section of the TMRC. The cross section of the TMRC at target level has been divided into a rectangular grid of 1 cm³ scoring cells to create this plot. The anisotropy of the energy spectrum in its angular dependence becomes particularly transparent due to contour lines added to both graphs of Fig. 3.

The statistical error in Fig. 2 is below 5% in the interval 0-90 degrees and about 10% in the interval 90-180 degrees. It becomes evident from these results that the high energy hadron radiation is strongly anisotropic in its angular distribution and that high energy hadrons (>100 MeV) which constitute the most significant problem in the shielding design appear predominantly in a rather small cone around the forward direction of the incident proton beam (see also Fig. 3a). Low energy neutrons display a nearly isotropic angular distribution, which is not presented in this figure.

Finally, we compare our results with data generated by FLUKA99 the other major MC particle transport code, which is widely used at CERN. This code treats nuclear inelastic interactions above 20 MeV within the pre-equilibrium cascade model PENAUT [13]. To treat the particle transport below 20 MeV, the FLUKA99 code employs cross section data which are based on the ENEA neutron cross section library [7]. In these calculations the statistical error is up to 15% in the angular interval 0-90 degrees and below 40% otherwise. The reason for this greater error in comparison to the MCNPX calculations are prohibitive computing times of our FLUKA99 implementation which has not been optimized to our LINUX-PC installation. Nevertheless, Fig. 4 demonstrates a surprisingly good agreement between MCNPX and FLUKA99 results despite the quite different physical models and nucleon cross section databases implemented in these two codes. There is certainly a systematic difference to be observed as FLUKA99 gives (particularly below 100 MeV) a slightly higher hadron

current leaking through the TMRC surface. The gross difference is about +10% for neutrons and about +20% for protons in the energy range considered here.

The transport data of hadrons leaving the TMRC surface are saved on file and later on used as source particles in the detailed analysis of computational strategies necessary for design of the biological shield.

III. Shielding Design

It is the purpose of this section to develop a strategy for the design of the biological shield of the target station in its spatial dimensions and material composition in order to meet direct radiation criteria outside the shield's surface under normal conditions of operation. Moreover, the biological shield should be of minimum size and weight, it should be geometrically compact and easily be constructed. We discuss different shielding configurations of the target station (including a standard double-layered shield as well as a 'sandwich' option consisting of a multiple of iron-concrete layers) on the basis of the results of our MC simulations.

III.1 Strategy for a 3D-Monte Carlo Simulation

In a first step in the realization of acceptable neutron source statistics, the results obtained for the neutron leakage at the surface of the TMRC have been parameterized in energy, position, and flight angle. The neutrons penetrating the inner surface of the shield as source particles of our MC simulation are then generated on the basis of such a parametrization. Furthermore, numerous preliminary calculations revealed that the dose rate on the outer surface of the biological shield in a given direction relative to the incident proton beam is affected by neutrons emitted from the TMRC surface only with energies greater than 1 MeV and within a radiation cone centered around the direction of interest having an opening angle of 60 degrees. Fig. 5 sketches the geometrical layout in the forward direction of the incident proton beam. The top of the radiation cone is placed right at the geometrical center of the TMRC. The source neutrons for the deep penetration calculation are then sampled from the cross section of the TMRC's surface with the radiation cone. This cross section is divided into three areas of same size and uniformly distributed source particles are then sampled from these areas using the parameterized source data. Furthermore, in order to achieve an adequate statistical significance of high energy source neutrons which are only infrequently generated, a source particle biasing in the energy domain has been applied. All other source hadrons in the energy region above 10 MeV are started as they appear at the surface of TMRC (i.e., no parameterization of the relevant transport data).

In shielding design incident source particles have to be traced down to thermal energy but it is also necessary to allow for spallation processes to occur in the shielding material because of the high energy source particles emitted by the TMRC. All this requires the use of biasing techniques to assure suitable statistical significance throughout the calculated particle energy spectra as well as to allow for acceptable computer times. A combination of two biasing techniques proved to be most successful: (i) energy dependent weight windows and (ii) source energy biasing. A weight window is a space-energy-dependent splitting and Russian roulette technique in which each space-energy phase-space cell defines a window of acceptable particle weights. If this weight is below a lower bound, Russian roulette is played and the particle is eventually eliminated. If, on the other hand, the particle is above the upper weight limit, the particle is split in such a way that all split particles are again within the weight window.

The biological shield itself consists typically of a single or multi-layer combination of iron followed by concrete. As typical shielding materials, magnetite concrete and low carbon steel were selected. The elementary composition with corresponding densities for these two materials is presented in Tab. I. In our first model (Model 1) the target station shield consists of an inner iron core surrounded by an outer concrete layer. The layout and dimensions are presented in Fig. 6 and Tab. II respectively. Fig. 6 also shows how the shield was divided in sections for the actual calculations. This division depends, of course, on the combination of biasing techniques chosen, and for a 3-dimensional shielding design it is reasonable to divide the geometry into spherical cells. Therefore, in our example the shield was divided into concentric spherical shells of an incremental radius of 25 cm.

The parameters for the energy dependent weight windows which are assigned to the spherical shells (Fig. 6) have been obtained from an empirical three-step procedure. (1) Geometry sampling: Geometry importances are assigned to the different cells in such a way that an approximately constant track density with increasing penetration depth is maintained. (2) Spatial weight windows which are independent of the particle energy are then introduced with bounds inversely proportional to the geometry importances because this ensures a roughly constant mean score of any track [14]. (3) Finally, the energy dependent weight windows are then adjusted in an iterative procedure in a way that the track density distribution is kept constant in any energy region with increasing penetration depth. Fig. 7 presents the lower weight bounds of the weight windows attached to the shells shown in Fig. 6. The ratios between upper and lower weight bounds are kept constant through the geometry.

Particular care was taken to match the space-energy weight windows at those boundaries where the equilibrium neutron spectrum is disturbed due to changes in the shielding material. Calculation efficiency was also increased by space-dependent energy cutoffs which allow to terminate particle tracks of negligible influence on the dose-rate outside the shield. Finally, to insure the correct treatment of spallation processes, the pre-equilibrium model following the intranuclear cascade has been activated. Furthermore, to consider properly backscattering processes, regions of 30 cm thickness behind the TMRC surface were taken into account. All photons generated by neutrons within the shield were transported and traced.

III.2 Deep Penetration Characteristics

Fig. 8 presents the results of a MCNPX calculation in which the strategy presented in the previous section has been utilized. What is shown is the energy distribution of neutron flux densities down to thermal energies for positions inside and outside the iron-concrete shield configuration (475 cm iron and 50 cm concrete in the forward direction). The figure presents results in the forward direction with respect to the incident proton beam. The statistical fluctuations are below 5% for each energy interval. The scoring zones are cylindrical cells of 75 cm diameter placed inside the various cylindrical shells and a track length estimator was used to calculate the neutron flux density per incident proton, per unit lethargy and per unit area.

The figure shows clearly the attenuation of the neutron spectrum with increasing shield thickness and the major energy component shifts towards the low energy region mainly due to elastic scattering and due to the 24 keV resonance of iron. Because of the inelastic scattering of high energy neutrons in the iron layer the low energy neutron flux spectrum (particularly below a few hundred keV) attenuates slower than its high energy tail. Therefore, low energy neutrons generated by the TMRC contribute only negligible to the neutron spectra deep within the shield and the chosen energy threshold of 1 MeV for the source neutrons is obviously

justified. The influence of the concrete component in absorbing low energy neutrons for > 475 cm is also nicely depicted in Fig. 8 (line Nr. 5). At $r \approx 500$ cm the spectrum is already close to a $1/E$ distribution.

Finally, Fig. 9 presents a comparison with FLUKA99 calculations for neutron energies > 0.1 MeV. There are some systematical differences in the energy distribution of the neutron flux. In the high energy region, at $r > 500$ cm, FLUKA99 reports a neutron flux which is higher by about 30% than the MCNPX result. On the other hand, in the energy range below 1 MeV the neutron flux is below the MCNPX result by almost one order of magnitude. These differences can probably be explained by differences in the cross-section libraries used by FLUKA99 and MCNPX.

III.3 Dose Rates and Attenuation length

Neutron dose equivalent rates have been calculated by folding the local neutron fluence with appropriate fluence-to-dose-equivalent conversion factors taken from the neutron ambient dose conversion coefficients based on the ICRP74 recommendations [15] which cover neutron energies up to 200 MeV. To higher neutron energies the conversion data have been augmented from data by Sannikov and Savitskaya [16]. Conversion factors for photons are given by A. Ferrari [17]. In actual MCNPX calculations these conversion factors simply constitute a response function for the appropriate tally.

For all model configurations of the biological shield discussed here we assumed a 5 MW incident proton beam (average current of 3.75 mA, or 2.34×10^{16} protons/s [18] at 1.334 MeV). As a first example we study the shield (Model 1) consisting of an inner steel layer (475 cm thick in the forward direction) and an outer concrete layer (50 cm thick). The neutron equivalent dose attenuation across the shield is presented in Fig. 10 for three different directions, namely 0, 45, and 90 degrees relative to the proton beam. Please note, that because of the anisotropic distribution of the source particles on the TMRC surface in 45 degrees 450 cm iron and in the 90 degrees direction only 425 cm iron is needed to get an ambient neutron dose rate the person is exposed to significantly below the design criterion of $5 \mu\text{Sv/h}$. According to Tab. II, which summarizes our results for the horizontal geometry of the shield there is a difference of 1 m in the thickness of the iron shield in going from forward to backward direction of the incident proton beam. In Fig. 10, the solid lines correspond to the 'total' neutron dose rate while dashed lines are used to show the dose rate due to 'high' energy neutrons (> 10 MeV). In general, the neutron dose decreases exponentially with increasing thickness of the iron layer. The same holds for the dose rate due to high energy neutrons but it is falling more steeply. The characteristics are quite similar in the different directions. It becomes also apparent that due to the build up of low energy neutrons (Fig. 8) in the iron layer the dose rate is dominated by the contributions of low energy neutrons in the outer regions of this iron layer. In the low energy region concrete has a higher shielding performance than iron due to the elastic scattering effect of hydrogen contained in concrete. Therefore, it is then the purpose of the outer concrete layer to reduce quite effectively the dose rate contribution of low energy neutrons. This becomes particularly transparent in Fig. 11 in which we compare the attenuation of the dose per incident proton in $\mu\text{Sv} \times \text{m}^2 / \text{p}$ as a function of the distance from the inner shield surface for different multi-layer models in the direction of the incident proton beam. The different shield configurations investigated in this study are compared in the Tab. II. For the second model (Model 2) which consists of an inner iron shield (425 cm) and an outer concrete layer (100 cm), the solid line without crosses in Fig. 11, corresponds to the 'total' neutron dose, while the corresponding dashed line represent the 'high energy' dose. The latter shows a steep exponential decay within the iron layer and a

slightly flatter decay within the concrete part. The total dose decays exponentially but with a smaller exponent until the concrete layer has been reached. Inside this layer we see a sharp drop in the local dose rate which turns into a much flatter decay at about 70 cm concrete. This is to be compared with the results for Model 1: 475 cm iron and 50 cm concrete in the direction of the incident proton beam. The solid line represents the total and the dashed line the high energy part of the dose rate. There is, of course, no difference between the two models up to the distance of 425 cm. The total dose rate follows then its previous course until the end of the iron layer is reached. We observe the sharp drop in the concrete layer which is now not fully utilized in its shielding potential because it ends already after 50 cm. In Model 3 we studied a 'sandwich' configuration: a 325 cm thick iron layer is followed by 50 cm concrete, then there is a second iron layer, 100 cm thick, and a final outer concrete layer with a thickness of 50 cm. This configuration results in about the same ambient dose and thus has no advantage over the much simpler two layer configurations. Table III summarizes our results for the neutron ambient dose equivalent rates for all the three models considered in this study. It is clear from the table that the concrete layer should be about 1 m thick to take full advantage of the low energy neutron absorption in the concrete layer.

Using the results of Fig. 11 it is easy to determine the neutron attenuation length in iron and in concrete. For distances beyond 200 cm from the inner surface the transmission curve becomes exponential, i.e. the neutron spectrum has reached its equilibrium. Thus, we use the results in the region 200 - 400 cm from the inner surface to estimate the attenuation length λ for iron, and the region beyond 450 cm for concrete. The values of the calculated dose equivalents multiplied by the square of the penetration depth were fitted with an exponential function and Table IV lists our results of the neutron attenuation lengths for the total and for the high energy (>10MeV) spectrum of neutrons generated by the 1.334 GeV incident proton beam. These numbers are of quite some importance in comparing our results with other model calculations or experiments. The literature [19] gives an attenuation length of 19 cm in iron for secondary neutrons (>20 MeV) generated by 1.3GeV protons, which is in quite good agreement with our results.

We also have to remark that photons contribute a maximum of 2 % to the total dose rate for all configurations investigated here. The photons might be more important for lower energies of incident protons (see [20], where results are reported for a concrete shield in which neutron capture generates a high gamma component). The little photon contribution to the total dose equivalent may thus also be due to the fact that most of the shield is made of iron. Components coming from secondary protons have certainly some relevance in the forward direction of the incident proton beam. Thus, secondary protons have been transported in all calculations (in contrast to photons) but their contribution is only a few percent (<5 %) of the total dose rate which obviously is dominated by neutrons, as was to be expected.

Finally, it is evident from our results that the double-layer shield with an inner iron layer (max. 425 cm thick) and an outer concrete layer (100 cm thick) is economically the best choice of the three models investigated here. Nevertheless, all models fulfill the requirement of an ambient dose equivalent rate of less than 5 μ Sv/h.

IV. Conclusions

The applicability of three dimensional Monte Carlo simulation in the design of the biological shield of a high intensity neutron spallation source has been investigated. To be concrete we considered as an example the target-moderator-reflector complex of the European Spallation Source. The task can be divided into two major steps. In a first step the particle fluences in their spatial and energy distribution on the TMRC surface are to be calculated using a not too detailed model of this complex. This data constitutes the source of incident particles for shielding design. For optimum data handling the neutron source particle data are further on parametrized in energy, position and flight angle. The second step concerns the actual shielding design. Variance improving techniques as they are nowadays offered by all good MC computer codes are essential in achieving acceptable computing performance and are therefore a major part in the development of a design strategy.

Iterative refinement of the various variance improving methods finally results in a stable strategy for the calculations which then allows to study various design models with only little modifications of the basic setup. The techniques discussed here can easily be extended to design studies of biological shields of accelerators, beam dumps, and other high intensity, high particle energy installations.

In this study two of the most prominent MC computer codes, namely MCNPX and FLUKA99 have been employed. Despite major differences in the physical models and cross-section databases implemented in these two codes the final geometric layout of the biological shield is identical which is a quite satisfactory result.

Acknowledgment

This research was performed under the auspices of the Austrian Federal Ministry of Education, Science and Culture under contract No. GZ 308.978/1-III/B/8/99.

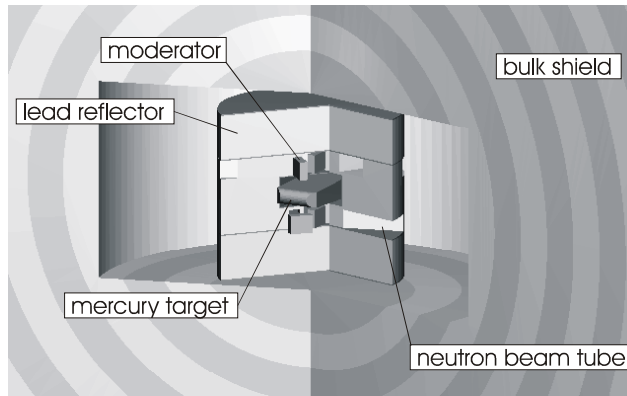


Fig. 1 Cutaway view of the TMRC geometry used in MC calculations to provide the particle source for the shielding design.

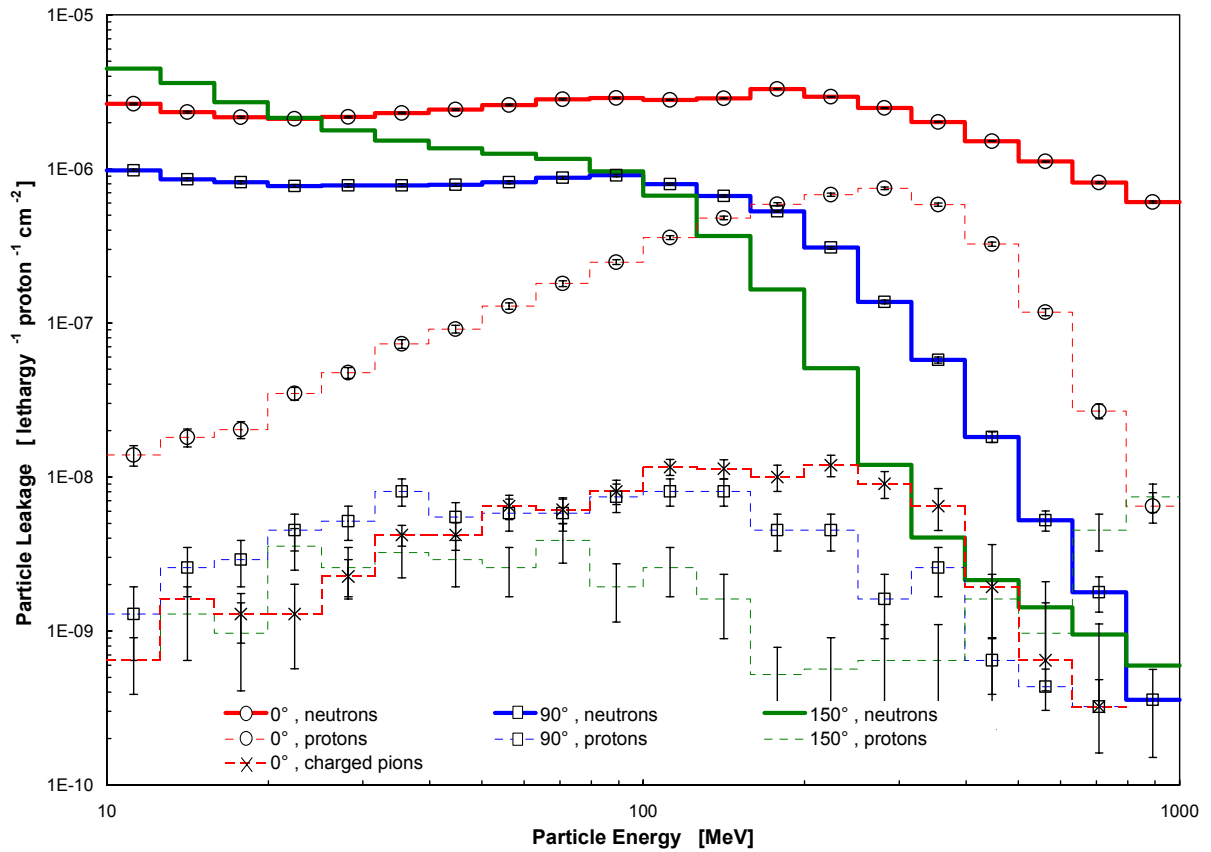


Fig. 2 Particle leakage per incident proton, unit lethargy and unit area on the outer surface of the TMRC for various directions with respect to the incident proton beam.

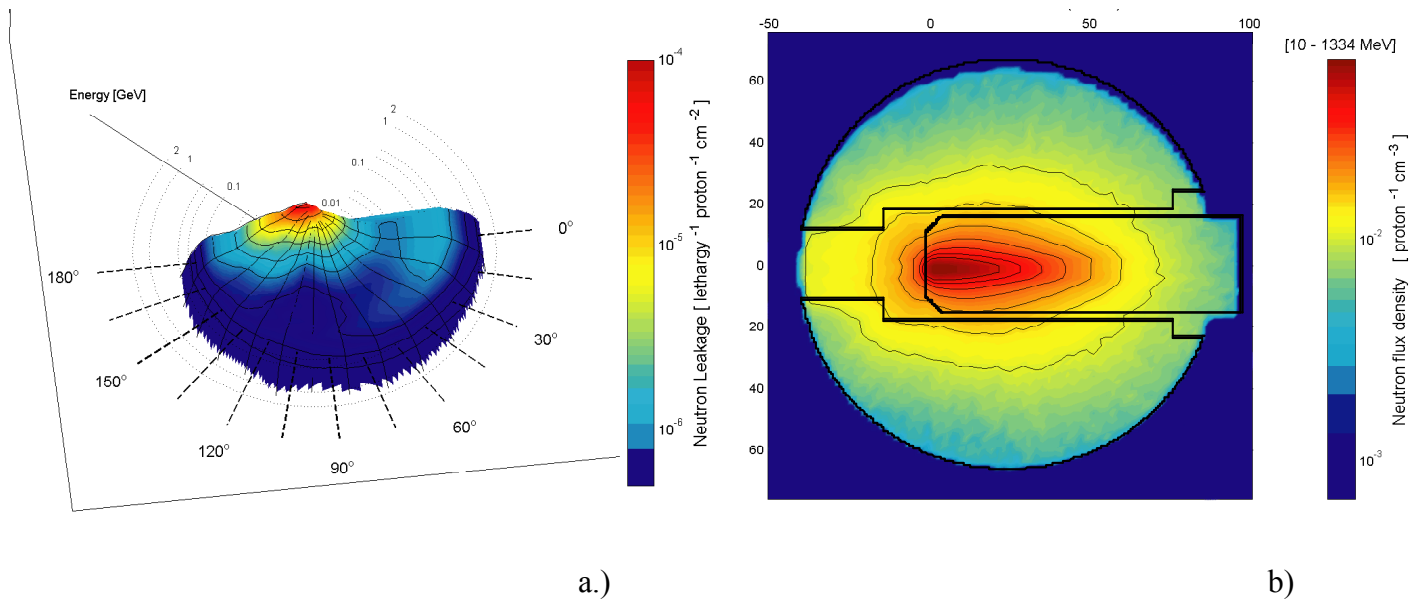


Fig. 3 a.) Angular distribution of the neutron leakage in neutrons per incident proton, unit lethargy and unit area at the outer surface of the TMRC for energies > 1 MeV.
 b.) Neutron flux density in neutrons per incident proton and per area unit along the transverse section of the TMRC. Axis units are given in cm.

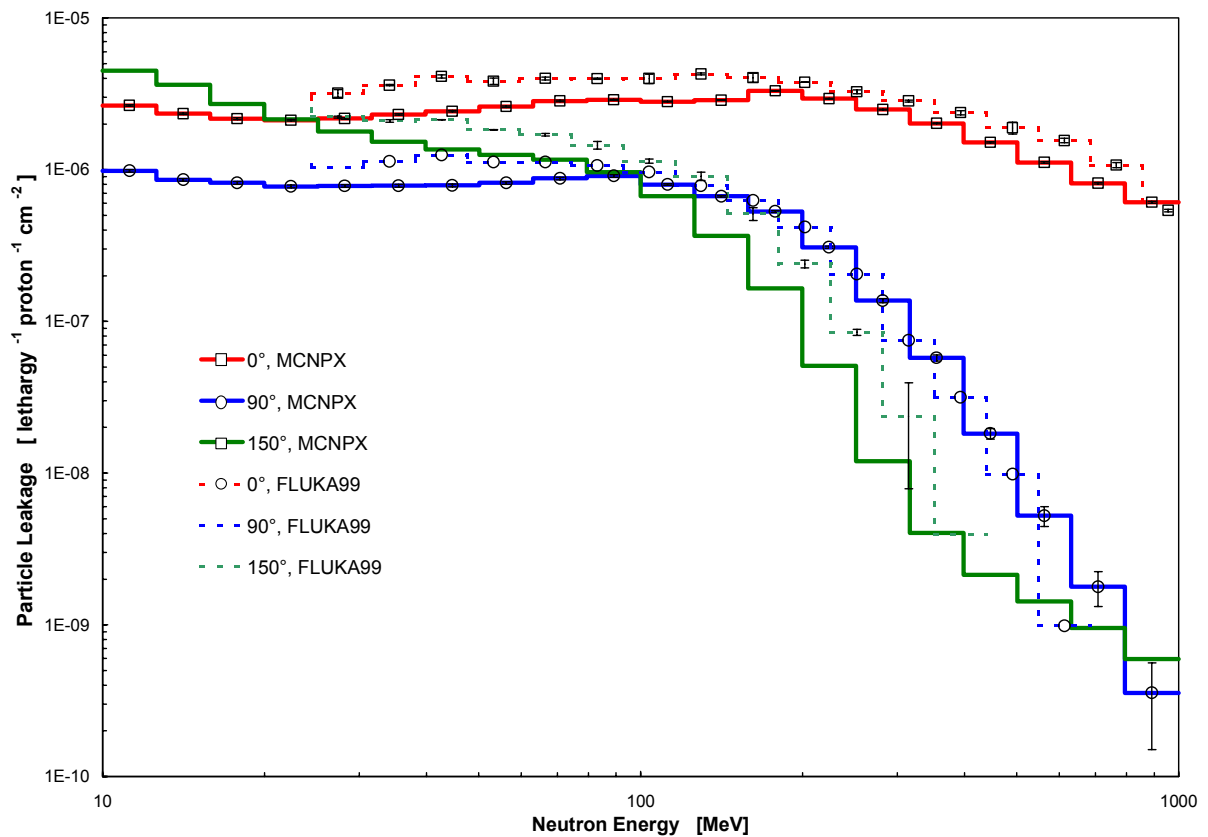


Fig. 4 Comparison between MCNPX and FLUKA99 results of neutron leakage spectra on the TMRC surface.

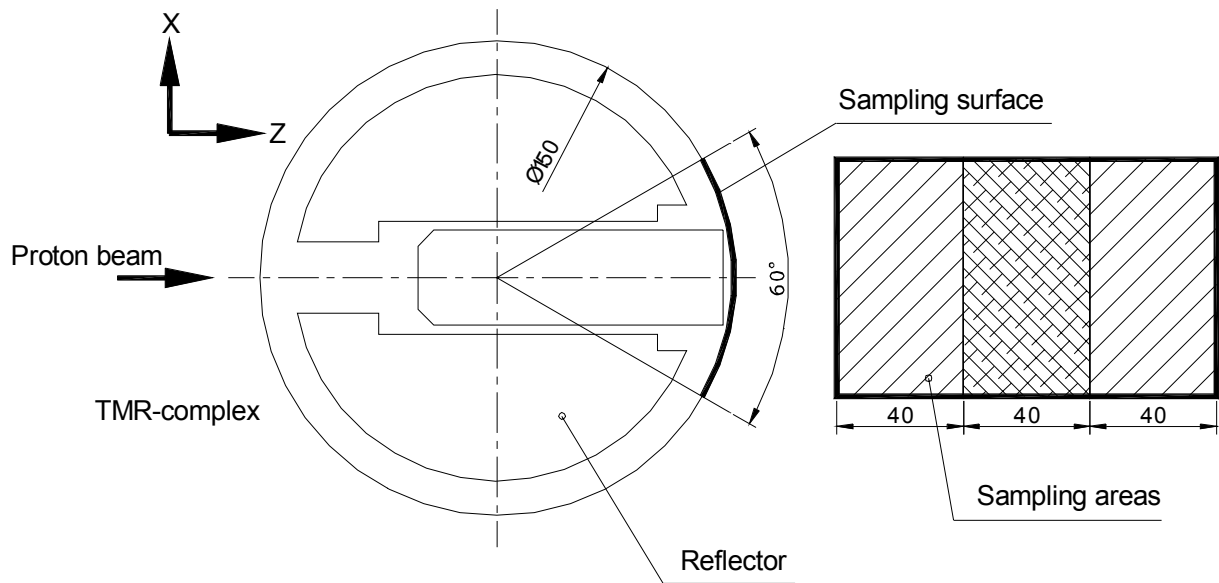


Fig. 5 Geometrical sketch of the sampling surface from which the start particles are emitted on the base of predetermined distributions. Dimensions are given in cm.

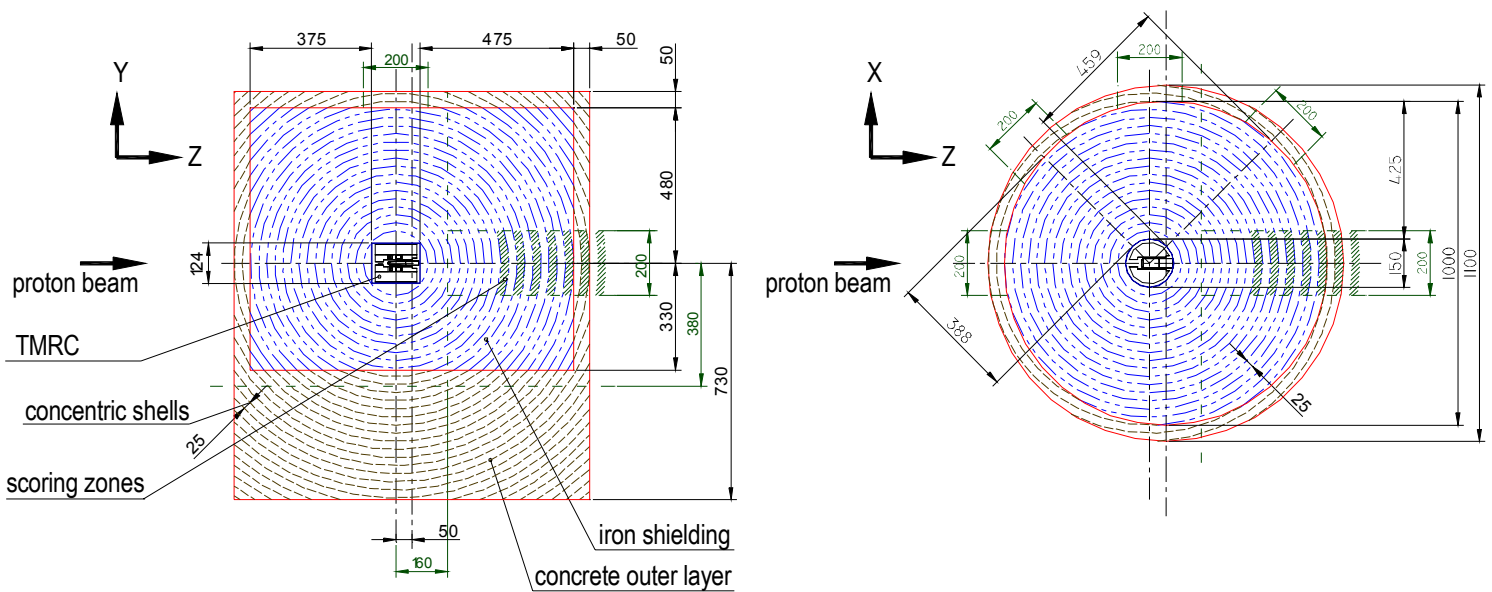


Fig. 6 Cross-sectional view of the model target station shield which consists of an inner iron core (475 cm thick in the proton beam direction) and an outer concrete layer (50 cm thick). All dimensions are given in cm.

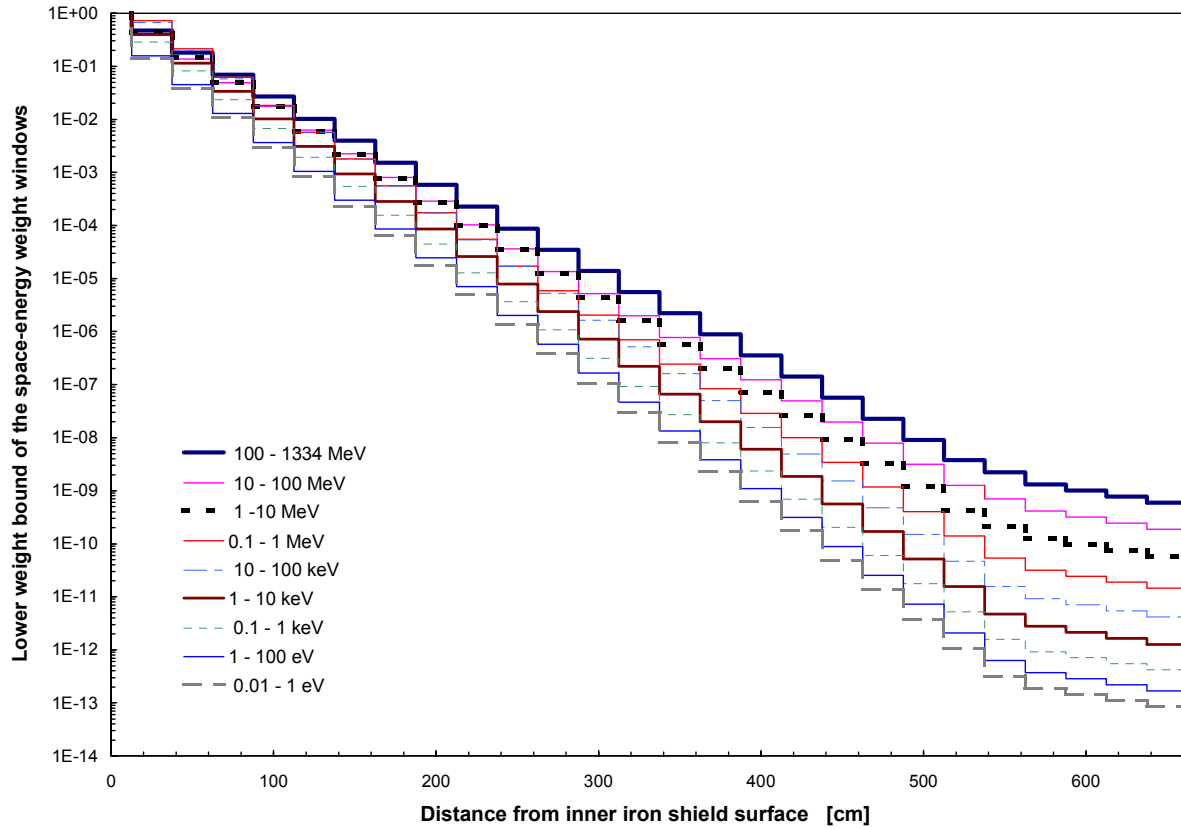


Fig. 7 Example of space-energy weight windows parameters for the forward direction as they were used in the shielding design.

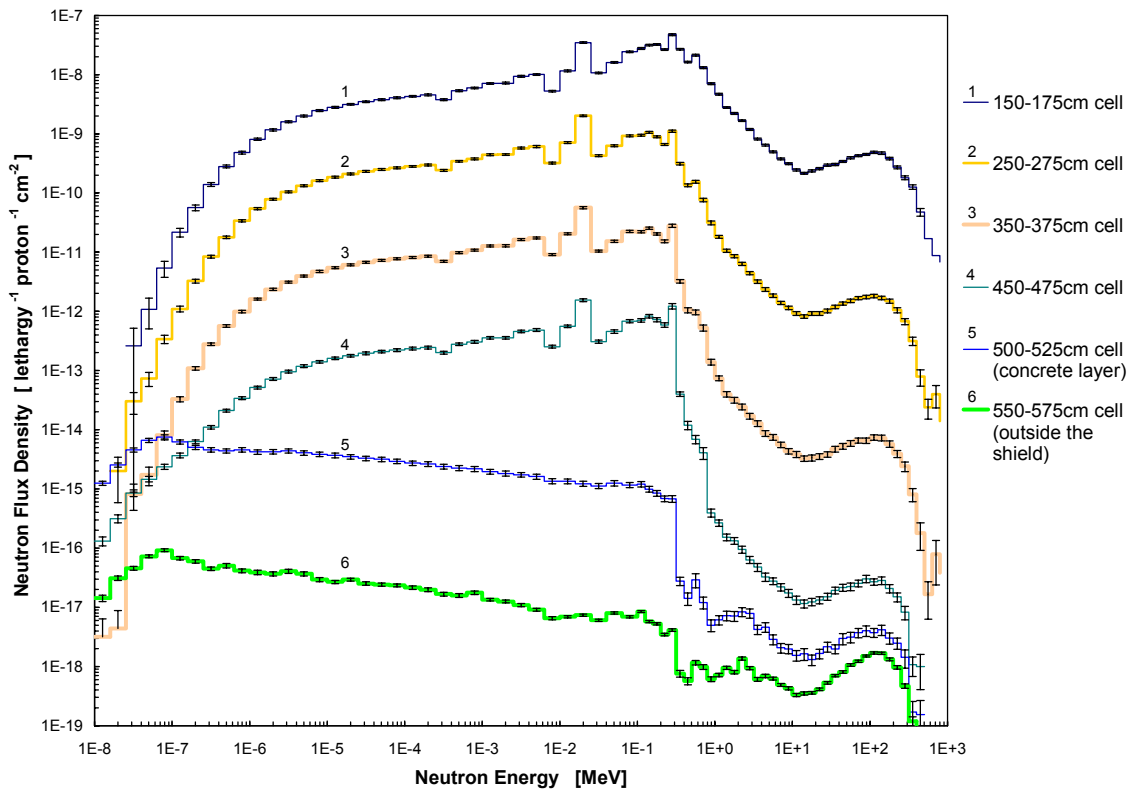


Fig. 8 Neutron flux density energy spectra for Model 1 (in neutrons per unit lethargy, incident proton, and unit area) across the shield in forward direction with respect to the proton beam.

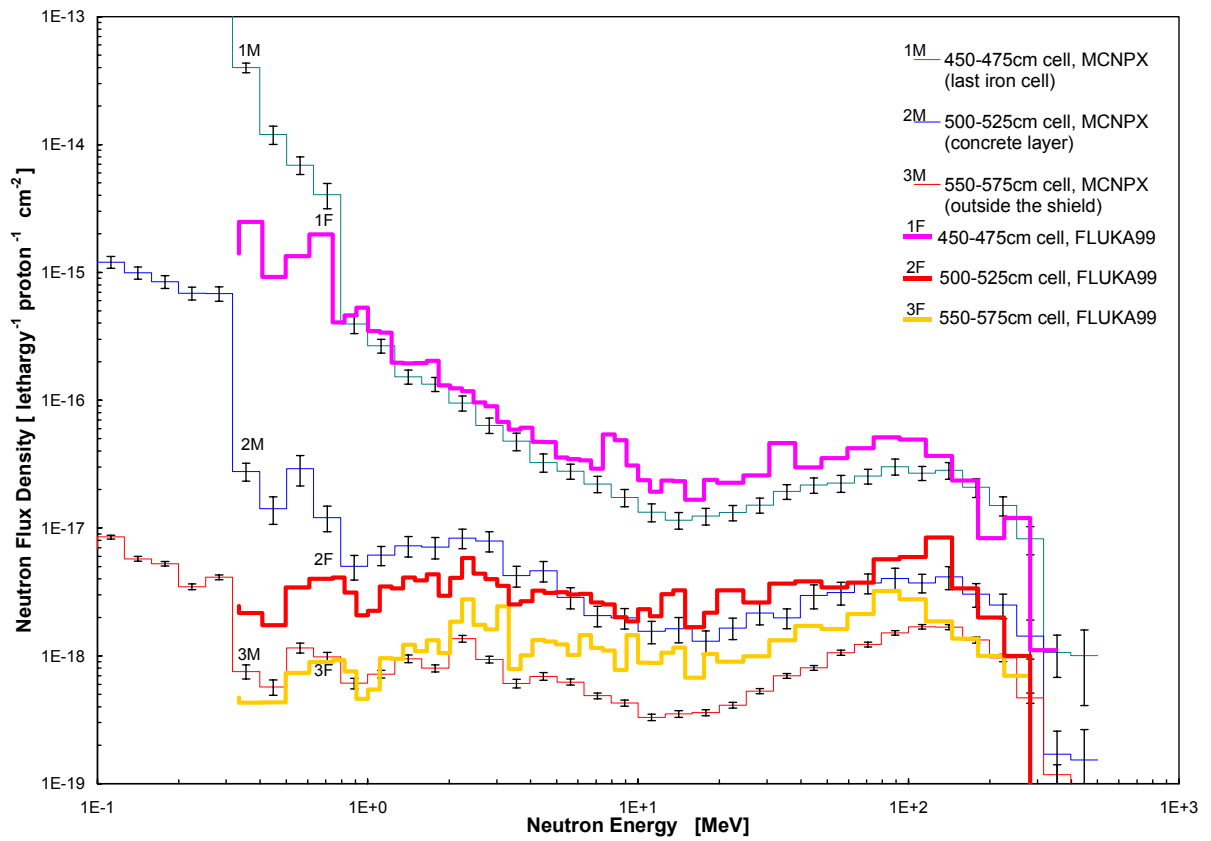


Fig. 9 Comparison of MCNPX results with FLUKA99 spectra for neutron energies > 0.1 MeV in the forward direction with respect to the incident proton beam for Model 1.

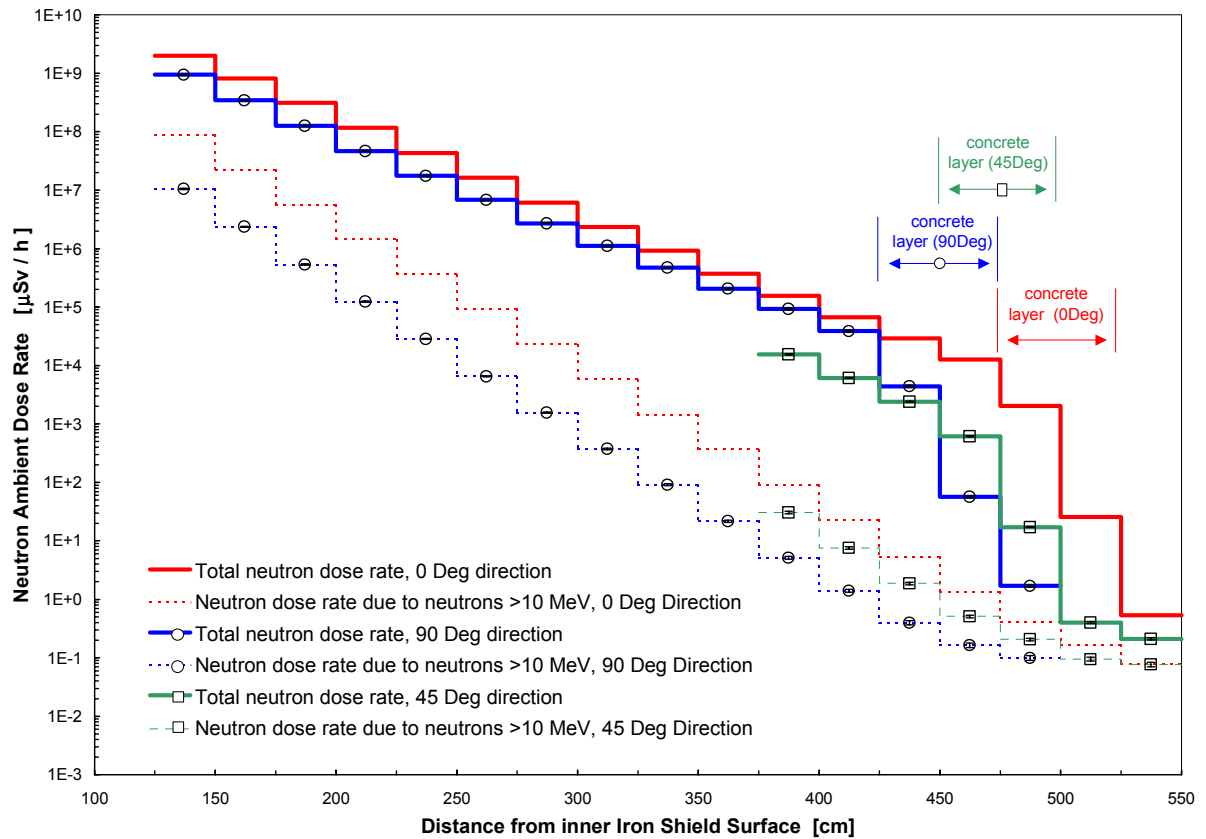


Fig. 10 Attenuation of neutron ambient dose equivalent in $\mu\text{Sv/h}$ along different directions across the shield (Model 1).

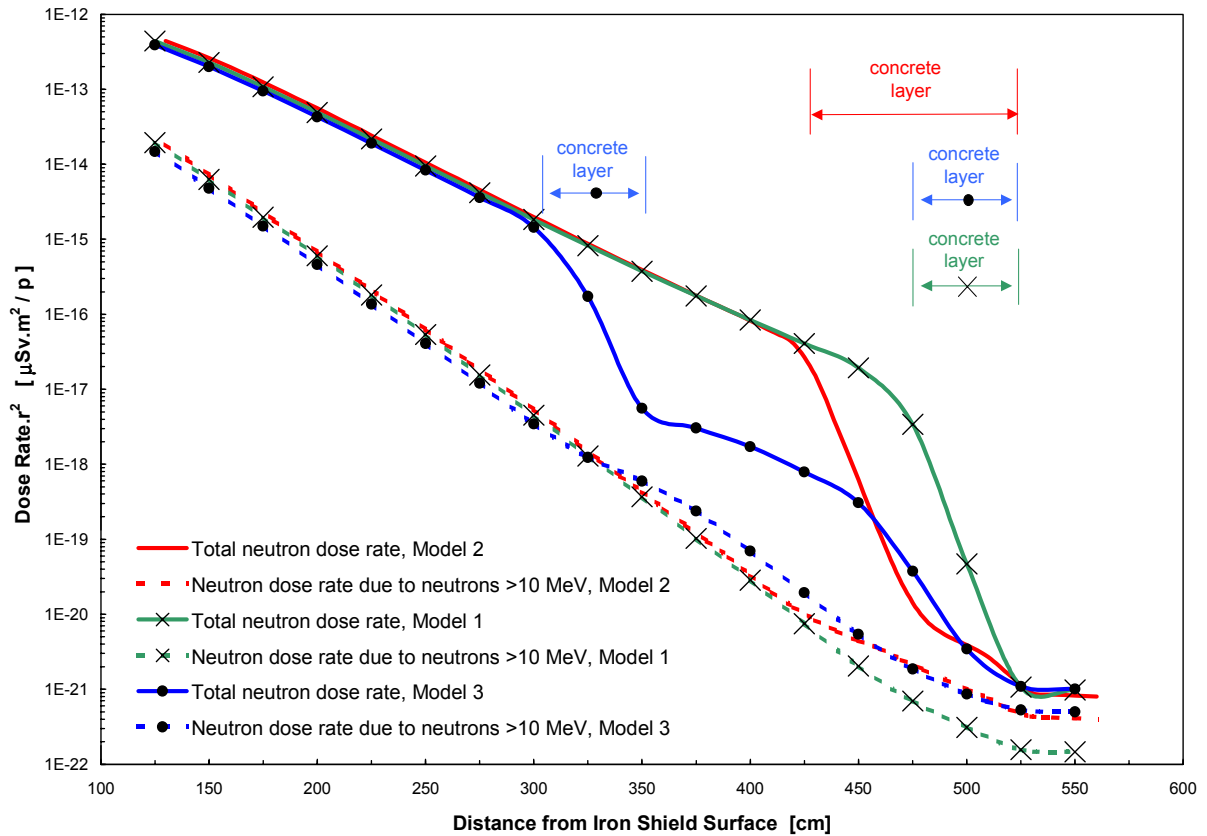


Fig. 11 Attenuation of neutron dose in forward direction as a function of the distance from the inner shield surface for various shield configurations.

Table I Elementary composition of the selected shielding materials.

Element	Low carbon steel (AISI 1019)	Magnetite concrete
	Weight per cent [%]	Weight per cent [%]
H	-	0.31
O	-	33.0
Mg	-	0.93
Al	-	2.34
Si	-	2.57
C	0.18	-
P	0.04	-
S	0.05	0.14
Mn	0.75	0.20
Fe	98.99	7.84
Ca	-	7.10
Ti	-	5.44
V	-	0.31
Cr	-	0.17
Density [g/cm ³]	7.84	3.53

Table II The investigated shield configurations with the appropriate layer thicknesses.

Shield configuration	Layer	Layer thickness in different directions [cm]		
		0°	90°	180°
Model 1 (double-layered shield)	iron	475	425	375
	concrete	50	50	50
Model 2 (double-layered shield)	iron	425	375	325
	concrete	100	100	100
Model 3 (double-layered shield in 'sandwich' type geometry)	iron	325	275	225
	concrete	50	50	50
	iron	100	100	100
	concrete	50	50	50

Table III Comparison of the neutron ambient dose equivalent rates at the shield's surface for the three models. The statistical errors associated to the results are below 5%.

Direction with respect to the incident proton beam	Shield thickness (cm)		Total neutron dose rate ($\mu\text{Sv/h}$)	High energy neutron dose rate ($\mu\text{Sv/h}$)	Contribution of the high energy to the total dose rate (%)
	Iron	concrete			
Model 1					
0°	475	50	0.8	0.2	25
45°	460	50	0.8	0.3	40
90°	423	50	2.0	0.3	15
180°	375	50	2.0	0.3	15
Model 2					
0°	425	100	0.75	0.6	80
Model 3					
0°	325 + 50 + 100 + 50		0.8	0.6	75

Table IV Attenuation of the neutron dose equivalent inside iron and concrete.

Energy range [MeV]	Neutron Attenuation length [cm]		
	Iron		Concrete
	0° direction	90° direction	0° direction
10 – 1334	22 ± 1	20 ± 1	38 ± 2
1E-8 – 1334 (total)	35 ± 1	31 ± 1	/

References

- [1] “National Spallation Neutron Source Conceptual Design Report”, NSNS/CDR-1/V1&2, Oak Ridge National Laboratory, Oak Ridge, TN (1997). See details in the home page at <http://www.sns.gov>.
- [2] “The European Spallation Source Study”, Vol.III, *The ESS Technical Study Report ESS-96-53-M, European Spallation Neutron Source*, (1996).
- [3] Furusaka, M., Ikeda, H.: “Overview of the Spallation Neutron-Source Project at JHF”, *Proc. 2nd Int. Topical Meeting on Nuclear Application of Accelerator Technology, Sept. 20-23, 1998*, Gatlinburg Tennessee, USA, 345 (1998).
- [4] Engle Jr., W.W.: “ANISN”, *Union Carbide Nuclear Division Report*, K-1693 ORNL-TN (1969).
- [5] Moritz, L.: “Using the Moyer Model at Energies less than 1 GeV”, *Proc. Of 9th Int. Conference on Radiation Shielding (ICRS-9), Oct. 17-22, 1999*, Tsukuba, Ibaraki, Japan, *Journal of Nuclear Science and Technology, Supplement 1*, 180 (2000).
- [6] Waters, L.S.: “MCNPX User’s Manual, Version 2.1.5”, Los Alamos National Laboratory, Los Alamos, NM, TPO-E83-G-UG-X-00001 (1999); <http://mcnpx.lanl.gov>.
- [7] Fasso, A., et al.: “FLUKA-99 User’s Manual” (2000), See details in the home page at <http://fluka.web.cern.ch/fluka/>
- [8] Prael, R. E. and Lichtenstein, H.: “User Guide to LCS: The LAHET Code System”, Los Alamos National Laboratory, Los Alamos, NM, LA-UR-89-3014 (1989).
- [9] Briesmeister, J. F.: “MCNPTM - A General Monte Carlo N-Particle Transport Code, Version 4B”, Los Alamos National Laboratory, LA-12625-M (1997).
- [10] Prael, R. E.: “A Review of Physics Models in the LAHETTM Code”, *Intermediate Energy Nuclear Data: Models and Codes, Proceedings of a Specialists’ Meeting*, Issyles-Moulineaux, France, 145 (1994).
- [11] Bertini, H.W., *Phys.Rev.* **188**, 1711 (1969).
- [12] Chadwick, M. B., et al.: “Cross Section Evaluations to 150MeV for Accelerator-Driven Systems and Implementation in MCNPX”, *Nuclear Science and Engineering* **131**, 293 (1999).
- [13] Fasso, A., et.al.: “FLUKA: performances and applications in the intermediate energy range”, *Proc. of an AEN/NEA Specialists’ Meeting on Shielding Aspects of Accelerators, Targets and Irradiation Facilities, 28-29 April 1994*, Arlington, OECD Documents (1995).
- [14] Both, E.B.: “A Sample Problem for Variance Reduction in MCNP”, Los Alamos National Laboratory, Los Alamos, NM, LA-10363-MS (1985).
- [15] ICRU Report 57: “Conversion coefficients for use in Radiological Protection Against External Radiation”, *International Commission on Radiation Units and Measurements*, Bethesda, Maryland, USA (1998).
- [16] Sannikov, A.V. and Savitskaya, E. N.: “Ambient Dose Equivalent Conversion Factors for High Energy Neutrons based on the ICRP 60 Recommendations”, *Radiation Protection Dosimetry* **70**, 383 (1997).
- [17] Ferrari, A., and Pelliccioni, M.: “On the Conversion Coefficients from Fluence to Ambient Dose Equivalent”, *Radiat. Prot. Dos.* **51**,251 (1994).
- [18] Filges, D., et.al.: “Nuclear Simulation and Radiation Physics Investigations of the Target Station of the European Spallation Neutron Source”, *Nuclear Technology* **132**, 30 (2000).
- [19] Hirayama, H.: “Intercomparison of Medium-Energy Neutron Attenuation in Iron and Concrete”, *Proc. Of the fourth Specialists’ Meeting on Shielding Aspects of Accelerators, Targets and Irradiation Facilities, 17-18 September 1998*, Knoxville, Tennessee, USA (1998).
- [20] Agosteo, S., et.al.: “Double differential distributions and attenuation in concrete for neutrons produced by 100-400 MeV protons on iron and tissue targets”, *NIM B* **114**, 70-80 (1996).